

# Stress-induced ordering of two-dimensional packings of elastic spheres

Zhenwei Yao\*

*School of Physics and Astronomy, and Institute of Natural Sciences,  
Shanghai Jiao Tong University, Shanghai 200240, China*

Packing of particles in confined environments is a common problem in multiple fields. Here, based on the two-dimensional Hertzian particle model, we study the packing of deformable spherical particles under compression, and reveal the crucial role of stress as an ordering field in regulating particle arrangement. Specifically, under increasing compression, the squeezed particles spontaneously organize into regular packings in the sequence of triangular and square lattices, pentagonal tessellation, and the reentrant triangular lattice. The rich ordered patterns and complex structures revealed in this work suggest a fruitful organizational strategy based on the interplay of external stress and intrinsic elastic instability of particle arrays.

## I. INTRODUCTION

Achieving order in the packing of elementary constituents in confined environments is an important problem arising in the study of simple liquids [1–3], amorphous solids [4–6], space tessellation [7–10] and especially in extensive soft matter systems such as the packing of granular materials [11, 12] and the self-assembly of colloids [13, 14], filaments [15, 16], and other supramolecular structures [17, 18]. To achieve ordered packing, several strategies have been proposed based on patterned substrates [19, 20], designed particle-particle interaction [14, 21, 22], chemical decoration of particles [23, 24], and electromagnetic fields [25, 26]. The resulting ordered patterns lay the foundation for the fabrication of new nano- and microstructured materials and provide broad possibilities of functionalization [27–29]. Especially, ordered two-dimensional (2D) arrays of particles on the surface lead to unique and intriguing properties [13, 30–32]. Recent studies on the phase behavior of 2D soft particle systems show the crucial role of volume fraction on ordered packing [33–35]. These studies inspire us to explore the role of stress in the packing of geometrically confined deformable particles. The imposed stress naturally reduces the free space available to particles, and it also introduces subtle kinetic effects on the microscopic elastic behavior of particles. These combined effects of stress may lead to an elasticity-based organizational principle for particle packing.

The goal of this work is to explore the role of stress as an ordering field in regulating particle arrangement. Our model consists of a collection of frictionless, spherical Hertzian particles confined in a two-dimensional box of tunable size. The soft particle model enables the variation of volume fraction beyond the hard-sphere limit, and soft particles also serve as artificial atoms to reveal fundamental processes in materials design across many length scales [33, 36]. This model system allows us to clarify a series of questions: How does order arise from

randomness under imposed stress? What kinds of order could be realized in the system of elastic particles? What is the microscopic behavior of defects in response to the external stress? To address these inquiries, we perform numerical experiment that allows us to track the detailed microscopic process in the movement of particles. The data are subject to the combined geometric, statistical and force analysis for extracting the essential physics. Here, we emphasize that in this work we focus on 2D packing. The three-dimensional (3D) packing problem is fundamentally different from the 2D case due to the intrinsic geometric frustrations [37, 38].

In this work, we reveal the scenario of how the collection of deformable particles adapt their relative positions to the squeezed space under compression. It is found that the highly heterogeneous local stress eliminates the randomness in the initial particle configuration, and guides the particles to form regular crystal lattices and quasicrystal structures. Specifically, the ordering of loosely packed particles is dominated by the entropic effect, and that of the squeezed particles under larger compression is determined by the minimization of elastic energy. We highlight the crucial role of the emergent grain boundary structure as an energy absorber to stabilize the triangular lattice, and the formation of square lattice resulting from a series of local elastic instability events. Under larger compression, we reveal the tessellation of deformable pentagons and the reentrant behavior. We also discuss the issue of reversibility and the kinetic effect of stress in facilitating ordered packing. This work illustrates the role of stress as an ordering field that may be exploited in various contexts of soft matter packing.

## II. MODEL AND METHOD

The model system consists of  $N$  identical elastic particles of mass  $m_0$  confined in a two-dimensional box of  $L_0 \times L_0$ . The initial particle configuration is generated by random disk packing that naturally creates inhomogeneity in density and stress distribution [39]. In the initial random disk packing, the particles of radius  $R$  are not in contact. To promote efficiency of simulation, we increase

---

\*Electronic address: zyao@sjtu.edu.cn

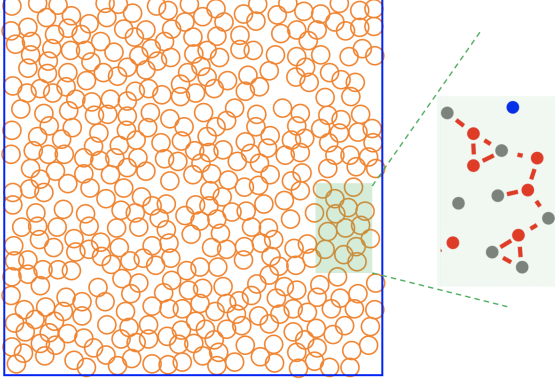


FIG. 1: Schematic plot of the model system. The circles represent elastic particles of uniform size. The initial state is generated by random packing of particles. In the zoomed-in plot, the colored dots represent different kinds of disclinations, and the red lines represent the contact force.

the radius of the particles in the initial state from  $R$  to  $R_0$ . The volume fraction and stress are thus controllable by specifying the radius  $R_0$  of the expanded particles. A typical random initial particle configuration is presented in Fig. 1. In our numerical experiment, the four walls of the box are simultaneously pushed inward, and the side length becomes  $L_0 - \Delta L$  in the final state. And the number density of the particles is  $\rho = N/(L_0 - \Delta L)^2$ . In each step of the compression process,  $L$  is reduced by  $\delta L$ , which is set to be sufficiently small to ensure that the system evolves quasi-statically.

The mechanical relaxation of the stressed system is governed by the particle-particle and particle-wall interactions, both of which are modelled by the Hertzian potential [36]. Specifically, the particle-particle interaction potential is

$$V_{pp}(r) = \begin{cases} \frac{\sqrt{2R_0}}{5D}(2R_0 - r)^{\frac{5}{2}} & r \leq 2R_0 \\ 0 & r > 2R_0, \end{cases}$$

where  $r$  the distance between the particle centers, and  $R_0$  is the radius of the particle.  $D = 3(1 - \nu^2)/(2E)$ , where  $E$  is the Young's modulus, and  $\nu$  is the Poisson ratio. The interaction potential between the particle and the rigid wall is

$$V_{pw}(r) = \begin{cases} \frac{2\sqrt{R}}{5D'}(R_0 - r)^{\frac{5}{2}} & r \leq R_0 \\ 0 & r > R_0, \end{cases}$$

where  $r$  the distance from the center of the particle to the wall, and  $D' = D/2$ .

With a given box size, we perform the steepest descent method to find the lowest energy state which corresponds to the optimal packing of the particles. Specifically, the particle configuration is continuously updated by simultaneously moving all of the particles along the direction of the force. The displacement is proportional to the magnitude of the force. The typical step size of the particle that is subject to the maximum force is  $s = 10^{-3}R_0$ .

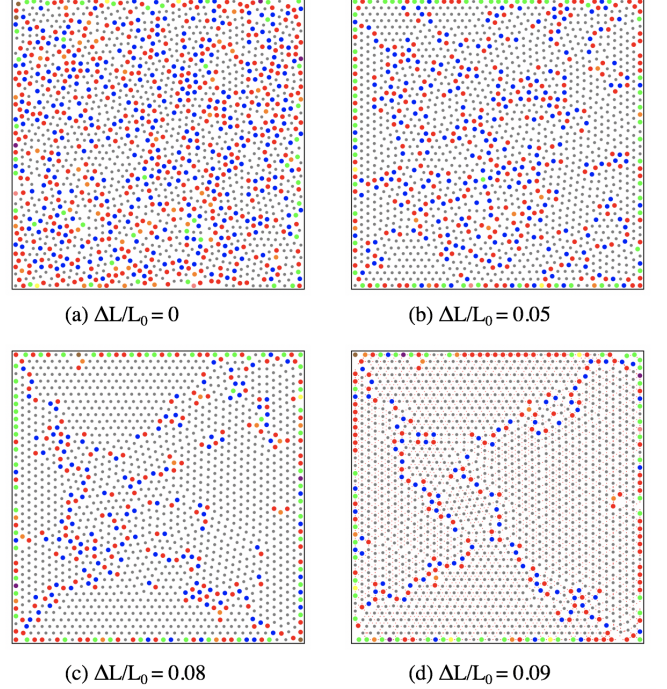


FIG. 2: Entropic ordering of random particle configuration into triangular lattice. All the configurations are in the lowest energy state. Each dot represents a particle. The red and blue dots are the five- and seven-fold disclinations. The total energy  $E = 0$  (a)-(c), and  $E = 1.12 \times 10^{-6}$  (d), which corresponds to a negligibly small overlap of particles. The compression rate  $\delta L = 0.1$ .  $\rho = 0.23$  (a), 0.25 (b), 0.26 (c), and 0.27 (d). The mean lattice spacing is 2.25 (a), 2.14 (b), 2.07 (c), and 2.05 (d).  $N = 1600$ .  $L_0 = 84$ .  $R = 0.7$ .

Evolution of the system is terminated when the slope of the energy curve becomes sufficiently flat. Typically, termination occurs if the reduction rate of the energy is less than 0.1% in ten thousand steps. In this work, we set  $R_0 = 1$ ,  $m_0 = 1$ , and  $D = 1$ . The units of length, time, and mass are thus  $R_0$ ,  $\sqrt{m_0 D / R_0}$ , and  $m_0$ . By denoting  $\tau_0 = \sqrt{m_0 D / R_0}$ , the unit of force is  $m_0 R_0 / \tau_0^2$ .

We resort to the combination of geometric, statistical and force analyses on the lowest energy particle configurations. Specifically, by Delaunay triangulation, one can identify different kinds of disclinations, which are elementary topological defect in two-dimensional triangular lattice [40]. An  $n$ -fold disclination refers to a vertex whose coordination number  $n$  is deviated from six. The crystallization process can be well characterized by tracking the evolution of the emergent disclinations. In the zoomed-in plot in Fig. 1, we show the five-fold (red dots) and seven-fold (blue dots) disclinations. The red lines between the dots represent the contact force. The magnitude of the force is indicated by the length of the line. We also analyze the diffraction pattern of the particle configurations calculated from the structure function [41]:  $S(\vec{q}) = \langle n(\vec{q})n(-\vec{q}) \rangle$ . The particle density  $n(\vec{x}) = \sum_{i=1}^N \delta(\vec{x} - \vec{x}_i)$ , and  $n(\vec{q}) = \sum_{i=1}^N \exp(-i\vec{q} \cdot \vec{x}_i)$ .

### III. RESULTS AND DISCUSSION

Figure 2 shows the growing region of triangular lattice as the system is slightly compressed. The particles are represented by dots, and the disclinations are indicated by different colors. The red and blue dots are the five- and seven-fold disclinations. Figure 2(a)-2(c) show the gradually established order in the arrangement of particles. Remarkably, the particles are free of overlap in this process. It indicates that spherical particles in a sufficiently crowded environment have the strong tendency of spontaneously forming a triangular lattice. In Fig. 2(d), the total energy is at the order of  $10^{-6}$ , which corresponds to an average overlap of particles as small as about  $0.01\%R_0$ . Therefore, the initial crystallization of particles is driven by entropy instead of energy, and it is known as entropic ordering [42]. The microscopic dynamics of this ordering process involves a series of defect events including disclination annihilation and dislocation glide [40].

Further compressing the system leads to the transition from triangular to square lattice. Scrutiny of the typical particle configurations presented in Fig. 3(a) and 3(b) reveals the crucial role of the grain boundary structure in resisting the increasing external compression and preserving the triangular lattice. A grain boundary in a two-dimensional lattice is a linear interface where crystallites of distinct orientations meet. Figure 3(a) shows that in the squeezed elastic particle system, the grain boundary as indicated by the blue curve consists of a series of empty pentagons. Under compression, these pentagonal voids shrink much faster than the lattice spacing in the crystallized regions. The quantitative result is presented in Fig. 3(e). It indicates that the grain boundary structure plays a dominant role in absorbing the volume reduced by the external compression. As the grain-boundary width shrinks, we also observe the drift of the entire grain boundary towards the left boundary as shown in Fig. 3(b); the light blue curve indicates the relative location of the grain boundary in Fig. 3(a). Here, the drift of the grain boundary structure is purely driven by external stress. Grain-boundary migration as driven by the competition between thermal energy and the tendency to minimize the grain-boundary curvature has been discussed in Ref. [43].

When the grain-boundary width is reduced to the size of the lattice spacing, a slight compression from  $\Delta L/L_0 = 0.37$  to  $\Delta L/L_0 = 0.38$  triggers the triangular-to-square lattice transition [see Fig. 3(b) and 3(c)]. The lattice transformation is initiated in a few random domains that are colored in green in Fig. 3(c). Note that all the particle configurations in Fig. 3 have reached the lowest energy state. The coexistence of the square and triangular lattices in Fig. 3(c) is a mechanically stable state. Further compressing the system leads to the extension of the square lattice to the entire system [see Fig. 3(d)].

To quantitatively characterize the triangular-to-square

lattice transition, we introduce the  $p$ -fold bond-orientational order parameter  $\Phi_p$  defined as [40]

$$\Phi_p = \frac{1}{N} \sum_{i=1}^N \left| \frac{1}{n_b} \sum_{j=1}^{n_b} \exp(ip\theta_{ij}) \right|, \quad (1)$$

where  $n_b$  is the number of neighbors surrounding the particle  $i$ ,  $\theta_{ij}$  is the angle between the line connecting the particles  $i$  and  $j$  and some chosen reference line,  $N$  is the total number of particles. The bond order in triangular and square lattices can be characterized by  $\Phi_4$  and  $\Phi_6$ , respectively. The dependence of  $\Phi_4$  and  $\Phi_6$  on  $\Delta L/L_0$  is presented in Fig. 3(f). With the increase of compression, the six-fold bond-orientational order emerges when  $\Delta L/L_0 > 0.1$ , and the triangular-to-square lattice transition occurs at  $\Delta L/L_0 \approx 0.4$ . Simulations of systems with  $N$  ranging from 100 to 2000 show that the critical values for the appearance of triangular lattice and the lattice transformation are independent of the number of particles. A further inquiry is if the formation of the square lattice is due to the square shape of the boundary. To address this question, we simulate systems with circular boundary, and also find triangular-to-square lattice transition, as well as the coexistence of triangular and square lattices as a mechanically stable configuration. The critical value for the triangular-to-square transition in the circular system is identical to that of the square system, as presented in Fig. 4.

In the triangular-to-square lattice transition, it is found that the distribution of contact force  $f$  is qualitatively changed.  $f$  is the magnitude of the force between two particles in contact. Statistical distributions of the magnitude of the contact force are plotted in Fig. 3(g) and 3(h) for the triangular and square lattices, respectively. We see that the lattice transformation leads to the split of the peak structure in Fig. 3(g). The separation of the contact force distribution is also seen in Fig. 3(b) and 3(d), where the length of the red lines represent the magnitude of the contact force. The short lines at the center of each square element in Fig. 3(d) correspond to the peak at the lower end of the force distribution in Fig. 3(h).

Here, we shall mention that the fabrication of square lattice generally involves anisotropic interactions. Various sophisticated schemes have been proposed to create anisotropic interactions, including design of particle shape and chemistry [23, 24, 44], application of electromagnetic fields [25] and capillary interactions [14, 22]. In our system, the triangular-to-square-lattice transformation is driven by the microscopic elastic instability of the squeezed particles under enhanced stress. This elasticity-based scheme may provide a general strategy in the broad contexts of soft matter packing like directed self-assembly and colloidal crystallization.

The triangular-to-square lattice transition can be understood by the following energetic calculation. Consider a collection of  $N$  particles in triangular and square lattices in a square box of side length  $L$ , respectively. Geometric argument shows that the total energies of these

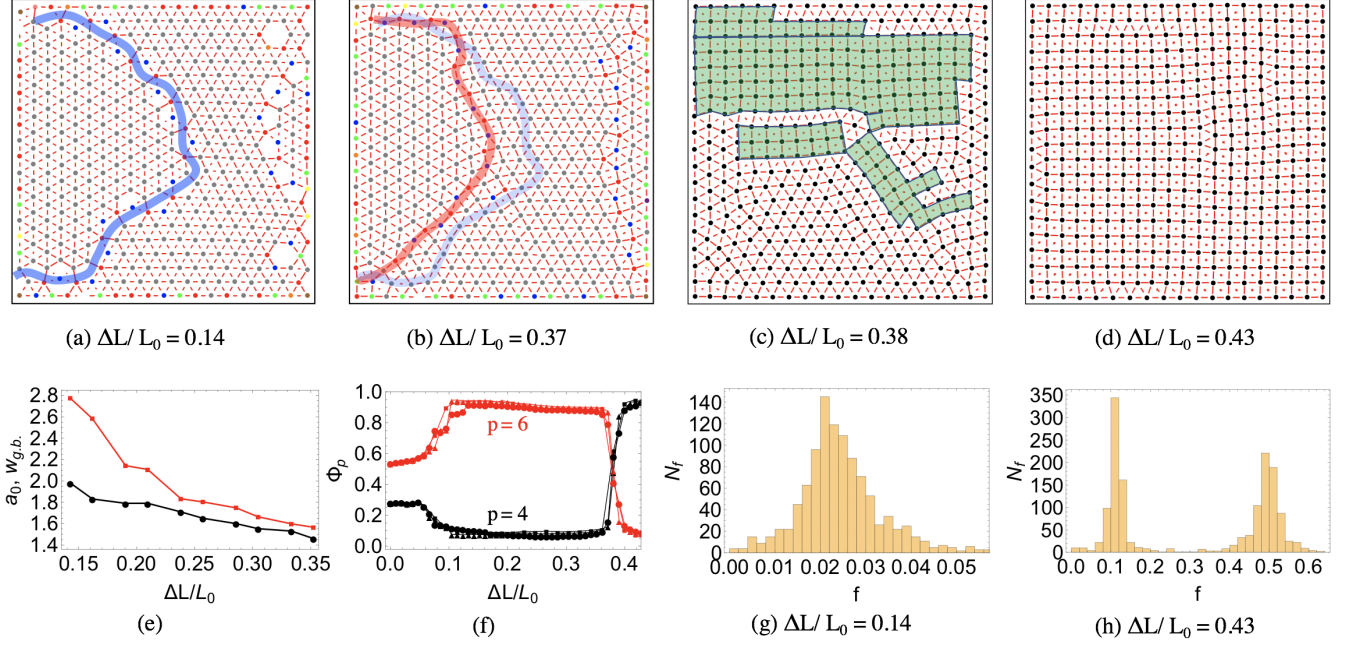


FIG. 3: Triangular- to square-lattice transformation under compression. (a)-(d) Lowest energy particle configurations as the compression proceeds. In (a) and (b), the red and blue dots are the five- and seven-fold disclinations. The red lines represent the contact force. The grain boundaries are indicated by the colored long curves. In (b), we also show the drift of the grain boundary with the compression of the system. In (c), the shadowed green domains indicate the square lattice in the background of the triangular lattice.  $\rho = 0.31$  (a), 0.57 (b), 0.58 (c), and 0.69 (d). The mean lattice spacing is 1.94 (a), 1.42 (b), 1.39 (c), and 1.29 (d). (e)-(h) Characterization of the lattice transformation. (e) Faster reduction of the grain boundary width (red curve with squares) in comparison with that of the lattice spacing (black curve with circles). (f) Quantitative characterization of the bond-orientational order of the crystal lattice by the order parameter  $\Phi_p$  (see main text for more information). The three sets of red and black curves are obtained at the compression rates of  $\delta L = 0.05$  (circles),  $\delta L = 0.1$  (triangles), and  $\delta L = 0.2$  (squares), respectively. (g) and (h) Splitting of the peak in the distribution profile of the contact force as the lattice transformation occurs.  $N = 400$ .  $L_0 = 42$ .  $R = 0.7$ .

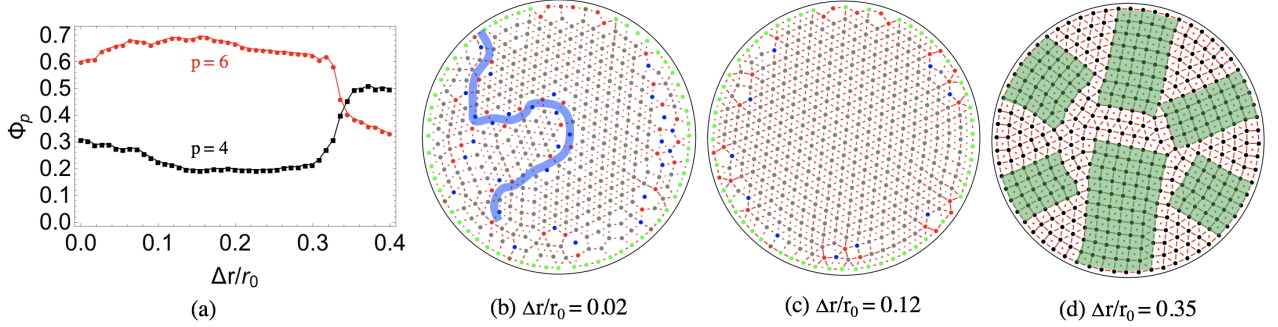


FIG. 4: Triangular- to square-lattice transformation of a circular system under quasi-static compression. (a) Variation of the bond-orientational order in the lattice transformation (see main text for more information). (b)-(d) Typical snapshots of lowest energy configurations as the compression proceeds. The colored dots represent different kinds of disclinations, and the red lines represent the contact force.  $r_0$  is the initial radius of the circular boundary.  $r_0 = 20.8$ . (b) The grain boundary in the triangular lattice is indicated by the blue curve. (d) The square lattice is colored green. The compression rate  $\delta r = 0.1$ .  $\rho = 0.96$  (b), 1.18 (c), and 2.17 (d). The mean lattice spacing is 1.94 (b), 1.75 (c), and 1.29 (d).  $N = 400$ .

two systems are:  $E_3 = 3N\epsilon_3$ , and  $E_4 = 2N\epsilon_4$ .  $\epsilon_3$  and  $\epsilon_4$  are the energy costs for a pair of particles in contact in the triangular and square lattices. When  $L < L_c$ ,  $E_4(L)$  becomes smaller than  $E_3(L)$ ; the system is thus dominated by the energetically favored square lattice. The

critical value  $L_c$  is derived as:

$$L_c = 2c_0\sqrt{N}R_0, \quad (2)$$

where  $c_0 = ((3/2)^{2/5} - 1)/(108^{1/20} - 1) \approx 0.67$ , and  $R_0$  is the radius of the particle. For  $N = 400$ , we have

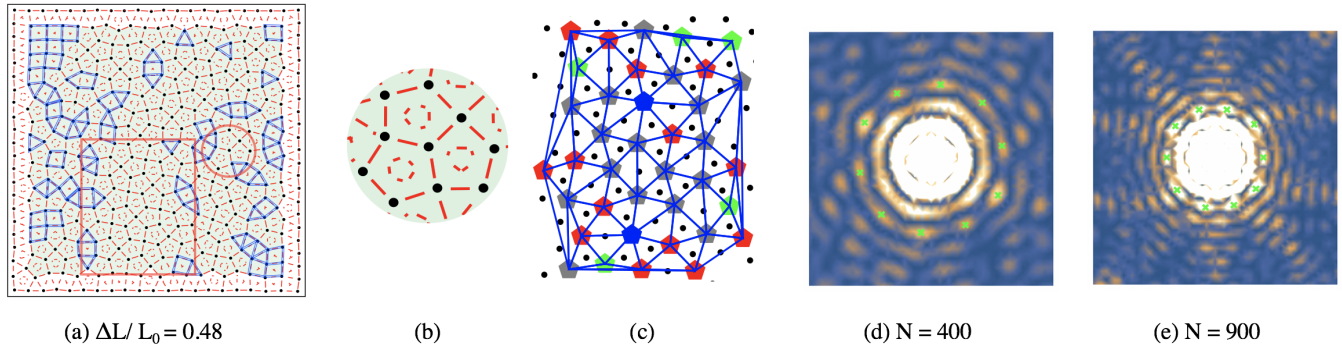


FIG. 5: Formation of quasicrystal structure as the compression proceeds. (a) Tesselation of space by triangles, squares (both enclosed by blue lines), and nonregular pentagons.  $\rho = 0.84$ . The mean lattice spacing is 1.2. (b) Zoomed-in plot of the region in the red circle in (a). The red lines represent the contact force. (c) Delaunay triangulation of the pentagons in the red square box in (a). The black dots represent the real particles. (d) and (e) Diffraction patterns of the pentagonal tessellation in the systems of  $N = 400$  and  $N = 900$  show the ten-fold rotational symmetry as indicated by the green cross marks.  $\delta L = 0.1$ .  $R = 0.7$ .

$L_c \approx 26.7$ . Simulations at varying compression rate (from  $\delta L = 0.05R_0$  to  $\delta L = 0.2R_0$  in each step) and initial particle radius  $R$  (from  $R = 0.5$  to  $R = 0.7$ ) return a common critical value of  $L_c \approx 26.0$ . These two critical values from numerical experiment and theoretical analysis are very close, and it shall be related to the friction-free feature of the particles that can facilitate the lattice transformation.

As the compression proceeds, the square lattice is transformed to a pattern as shown in Fig. 5(a). We observe the tessellation of space by the three kinds of elementary shapes: squares, triangles, and pentagons. The zoomed-in plot in Fig. 5(b) shows that each pentagon is characterized by five long red lines connecting the five particles and five short lines inside the pentagon. The short lines represent the contact of a particle with its next nearest neighbors around the pentagon. We emphasize that the introduction of contact force lines allows us to unambiguously identify the pentagonal units. Comparison of the straight contact force lines in the rectangular lattice in Fig. 3(d) and the zig-zag force lines in Fig. 5(a) shows that the pentagonal structures originate from the local elastic instability characterized by the buckling of the contact force lines. Figure 5(c) shows the packing of the emergent pentagonal units. The black dots represent real particles. Each pentad of particles is represented by a pentagon. Delaunay triangulation reveals the underlying topological structure. The red and blue pentagons indicate the five- and seven-fold disclinations in the triangulated pentagons. These pentagonal objects enrich the scenario of regular packing and 2D crystallography [30, 34, 45, 46].

The tessellation of a continuous flat region by pentagons is remarkable. As a geometric restriction, regular pentagonal tiling on the Euclidean plane is impossible. Regular pentagons can tile the hyperbolic plane and the sphere though [47]. Here, the key to achieving the pentagonal tessellation is the deformability of the pentagons

due to the softness of the particles [8]. The tessellation of deformable pentagons implies an induced non-Euclidean geometric structure in the particle array under high compression [48–50]. The nonregular pentagonal tessellation realized in soft particle arrays explains the extensive existence of quasicrystals in soft matter systems [34, 35, 51–53]. In our system, we reveal the ten-fold rotational symmetry in the diffraction patterns as a characteristic of a quasicrystal, which is indicated by the ten green cross marks in Fig. 5(d) and 5(e). It is in contrast with the eight- and twelve-fold rotational symmetries of quasicrystals found in unconstrained soft particle systems in Ref. [35].

The distinct rotational symmetries of the quasicrystal structures reported in Ref. [35] and that in our work suggest the subtle kinetic effect of external stress on the packing of soft particles, which is beyond merely changing the particle density. We notice that in our system crystallization is initiated at the boundary as the compression proceeds. To further illustrate the kinetic effect of the external stress, we examine the mechanical relaxation of randomly distributed particles in boxes of given sizes, and compare the resulting lowest energy configurations with those obtained via the compression procedure. In Fig. 6, the upper panels show the lowest energy configurations in a single gradual compression process. The lower panels show the corresponding lowest energy configurations upon the same amount of compression, but each of them is via the independent relaxation of random particle distribution. Comparison of these two kinds of cases clearly shows that imposing compression can significantly facilitate ordered packing, especially for the systems with relatively high particle density.

Under even larger compression, it is observed that the pentagonal tessellation becomes unstable, and the system returns to the triangular lattice, as shown in Fig. 7. This reentrant behavior can be attributed to the effect of density variation under compression [34, 54]. Scattered

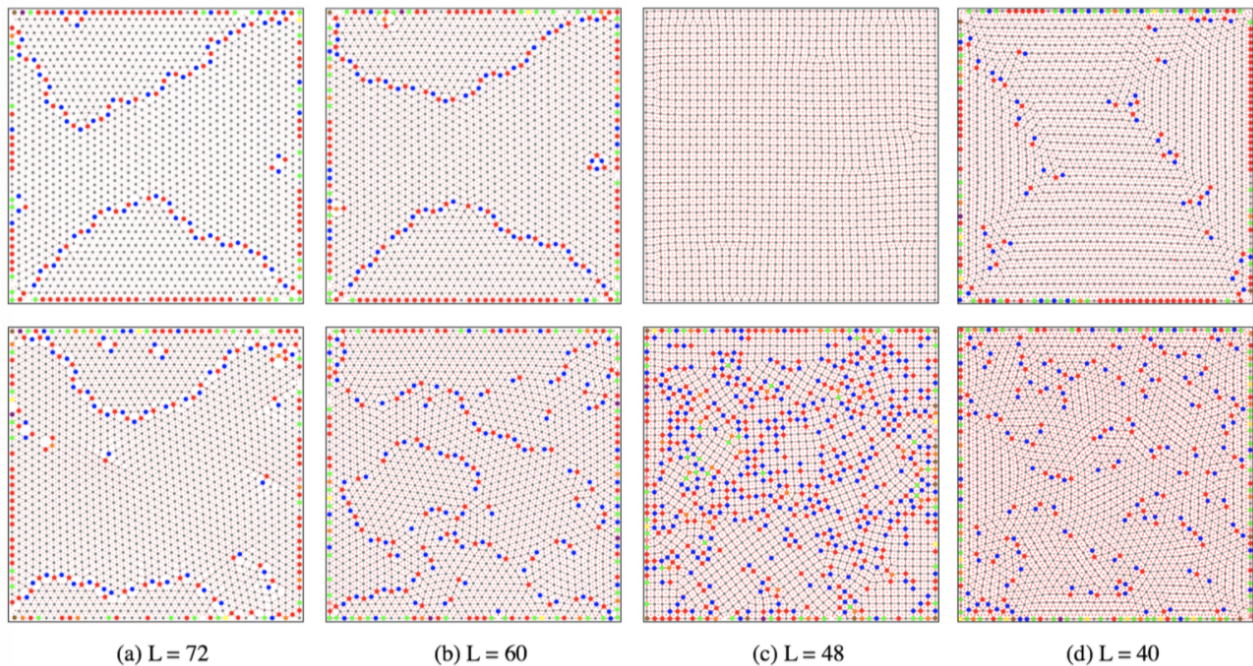


FIG. 6: Imposing compression significantly improves ordered packing of elastic particles, especially in the regime of high particle density. Upper panels: the evolution is driven by a single gradual compression process. The system is initially free of stress at  $L = L_0 = 84$ .  $\delta L = 0.1$ . Lower panels: lowest energy configurations via relaxation of randomly distributed particles in the boxes of given sizes. The colored dots represent different kinds of disclinations, and the red lines represent the contact force.  $N = 1600$ .

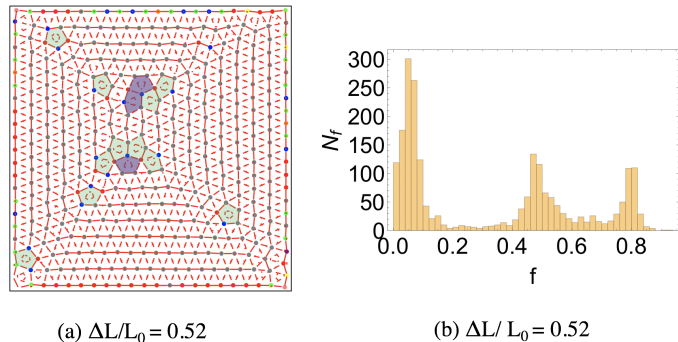


FIG. 7: Reentrant configurational transition to triangular lattice at larger compression. (a) The triangular lattice with scattered dislocational (green) and disclinal (purple) pentagonal vacancies. The red lines represent the contact force. (b) Further splitting of the peak in the distribution profile of the contact force as the lattice transformation occurs [in comparison with Fig. 3(g) and 3(h)].  $\rho = 0.98$ . The mean lattice spacing is 1.1.  $N = 400$ .  $\delta L = 0.1$ .  $L_0 = 42$ .  $R = 0.7$ .

dislocational (green) and disclinal (purple) pentagonal vacancies are observed in the triangular lattice. Pentagonal vacancies of distinct topological nature have been found in Lennard-Jones crystals confined on the sphere in our previous work [55]. Statistical distribution of the contact force in the configuration of Fig. 7(a) is presented in

Fig. 7(b). The number of peaks increases from two [see Fig. 3(h)] to three. Furthermore, the peaks experience rightward drift under enhanced compression. The close connection of contact force distribution and particle configuration suggests the contact-force analysis as a useful tool for revealing important structure information in deformable particle systems. Here, we shall note that high compression may be realized in a series of deformable mesoparticle systems, such as ultrasoft colloids and hydrogel beads [34, 56]. The Hertzian model, which is based on the linear continuum elasticity theory, may not quantitatively describe the relevant soft interactions [33, 34, 57]. The strong repulsion between two close particles is qualitatively captured by the Hertzian potential. As such, the numerical results in Figs. 5 and 7 present a plausible scenario of ordered packing of elastic particles under high compression.

We finally briefly discuss the robustness of the compression-driven ordered packing, the reversibility issue and role of dimension on particle packing. In our preceding discussion, we show that external compression eliminates the randomness in the initial particle configuration, and pushes the system to develop a series of ordered structures from triangular and square lattices [see Fig. 3] to pentagonal tessellation [see Fig. 5], and finally back to the triangular lattice [see Fig. 7]. In this process, as shown in Fig. 8, the system energy increases with  $\Delta L$  at a faster rate than the quadratic law, which indicates

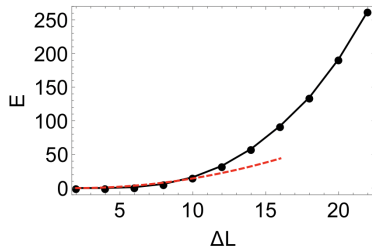


FIG. 8: Plot of total energy versus the amount of compression  $\Delta L$ .  $E$  is the energy of the relaxed particle configuration at a given box size  $L = L_0 - \Delta L$ .  $L_0 = 42$ . The red dashed curve is a quadratic fitting.  $\delta L = 0.1$ .  $N = 400$ .  $R = 0.7$ .

an enhanced rigidity of the system. Systematic simulations at varying compression rate ( $\delta L$  ranges from 0.05 to 0.2) and  $R$ -controlled initial stress level ( $R$  ranges from 0.5 to 0.8) reveal that the particle configuration always evolves by the same sequence. By reversing the compression process, could the system exhibit any memory effect? To address this question, we start from the triangular lattice under high compression, and gradually enlarge the box size. It turns out that the sequence of order is reversed. At the end of the cycle of compression and expansion, the initial randomness in the packing of particles is eliminated, and the system terminates at the stress-free triangular lattice. Our simulations imply that two-dimensional monodisperse elastic particles have the natural tendency to form ordered phases. This tendency can be attributed to the lack of geometrical frustration; the local dense packing is compatible with the global dense packing in the form of triangular lattice [37]. In contrast, a three-dimensional system is intrinsically geometrically frustrated, because the preferred local icosahedral structure cannot be extended to the whole flat

space [37, 38].

#### IV. CONCLUSION

In summary, by the Hertzian particle model, we have illustrated the crucial role of stress in organizing particles from random to ordered states in 2D packings. Specifically, we have revealed regular packings from triangular and square lattices to the remarkable quasicrystal structure, and to the reentrant triangular lattice under increasing compression. We have also identified the grain boundary structure as an energy absorber to stabilize the triangular lattice, and characterized the regular packing at high compression in terms of pentagonal tessellation. The physical origin of ordered packing is essentially from the interplay of external stress and intrinsic elastic instability of the particle array. In combination with the broad possibility of interaction potential design in soft matter systems, exploiting the role of stress as an ordering field may provide a new dimension for realizing ordered packings in various 2D cases like self-assembly and colloidal crystallization on interfaces. Due to the intrinsic geometric frustration in 3D systems that is absent in planar 2D systems, it is of interest to further explore the role of stress in regulating 3D packings that may lead to new physics not seen in 2D systems.

#### V. ACKNOWLEDGMENTS

This work was supported by NSFC Grants No. 16Z103010253. The author thanks the support from the Student Innovation Center at Shanghai Jiao Tong University.

- 
- [1] G. Scott, A. Charlesworth, and M. Mak, *J. Chem. Phys.* **40**, 611 (1964).
  - [2] J. Finney, *Proc. R. Soc. London, Ser. A* **319**, 495 (1970).
  - [3] J.-P. Hansen and I. R. McDonald, *Theory of Simple Liquids* (Elsevier, 1990).
  - [4] R. Zallen, *The Physics of Amorphous Solids* (Wiley, New York, 1983).
  - [5] E. R. Weeks, *Nat. Phys.* **11**, 381 (2015).
  - [6] A.-M. Philippe, D. Truzzolillo, J. Galvan-Myoshi, P. Dieudonné-George, V. Trappe, L. Berthier, and L. Cipelletti, *Phys. Rev. E* **97**, 040601(R) (2018).
  - [7] H. Wang, *Bell System Technical Journal* **40**, 1 (1961).
  - [8] P. Bowers and K. Stephenson, *Conform. Geom. Dyn.* **1**, 58 (1997).
  - [9] A. Okabe, B. Boots, K. Sugihara, and S. Chiu, *Spatial tessellations: concepts and applications of Voronoi diagrams*, vol. 501 (Wiley, 2009).
  - [10] E. Palatinus and B. Bánhelyi, in *Proceedings of the 8th International Conference on Applied Informatics, Eger, Hungary* (2010), pp. 255–262.
  - [11] M.D. Rintoul and S. Torquato, *Phys. Rev. Lett.* **77**, 4198 (1996).
  - [12] H. A. Makse, D. L. Johnson, and L. M. Schwartz, *Phys. Rev. Lett.* **84**, 4160 (2000).
  - [13] A. Dinsmore, M. F. Hsu, M. Nikolaides, M. Marquez, A. Bausch, and D. Weitz, *Science* **298**, 1006 (2002).
  - [14] D. Ershov, J. Sprakel, J. Appel, M. A. C. Stuart, and J. van der Gucht, *Proc. Natl. Acad. Sci. U.S.A.* **110**, 9220 (2013).
  - [15] H. Cui, E. Pashuck, Y. Velichko, S. Weigand, A. Cheetham, C. Newcomb, and S. Stupp, *Science* **327**, 555 (2010).
  - [16] I. R. Bruss and G. M. Grason, *Proc. Natl. Acad. Sci. U.S.A.* **109**, 10781 (2012).
  - [17] L. C. Palmer, Y. S. Velichko, M. Olvera de la Cruz, and S. I. Stupp, *Philos. T. Roy. Soc. A* **365**, 1417 (2007).
  - [18] W. Xu, Z. Xu, C. Cai, J. Lin, S. Zhang, L. Zhang, S. Lin, Y. Yao, and H. Qi, *J. Phys. Chem. Lett.* **10**, 6375 (2019).
  - [19] Y.-H. Ye, S. Badilescu, V.-V. Truong, P. Rochon, and A. Natansohn, *Appl. Phys. Lett.* **79**, 872 (2001).

- [20] S. L. Hellstrom, Y. Kim, J. S. Fakonas, A. J. Senesi, R. J. Macfarlane, C. A. Mirkin, and H. A. Atwater, *Nano Lett.* **13**, 6084 (2013).
- [21] G. Meng, J. Paulose, D. R. Nelson, and V. N. Manoharan, *Science* **343**, 634 (2014).
- [22] I. B. Liu, N. Sharifi-Mood, and K. J. Stebe, *Annu. Rev. Condens. Matter Phys.* **9**, 283 (2018).
- [23] C. Knorowski and A. Travesset, *Soft Matter* **8**, 12053 (2012).
- [24] Y. Li, H. Miao, H. Ma, and J. Z. Chen, *Soft Matter* **9**, 11461 (2013).
- [25] S. L. Biswal and A. P. Gast, *Phys. Rev. E* **69**, 041406 (2004).
- [26] P. Tierno, R. Golestanian, I. Pagonabarraga, and F. Sagués, *Phys. Rev. Lett.* **101**, 218304 (2008).
- [27] J. Zhang, Y. Li, X. Zhang, and B. Yang, *Adv. Mater.* **22**, 4249 (2010).
- [28] F. Li, D. P. Josephson, and A. Stein, *Angew. Chem. Int. Ed.* **50**, 360 (2011).
- [29] Y. Wang, Y. Wang, D. R. Breed, V. N. Manoharan, L. Feng, A. D. Hollingsworth, M. Weck, and D. J. Pine, *Nature* **491**, 51 (2012).
- [30] A. Bausch, M. Bowick, A. Cacciuto, A. Dinsmore, M. Hsu, D. Nelson, M. Nikolaides, A. Travesset, and D. Weitz, *Science* **299**, 1716 (2003).
- [31] D. Wan, M. J. Bowick, and R. Sknepnek, *Phys. Rev. E* **91**, 033205 (2015).
- [32] M. Brojan, D. Terwagne, R. Lagrange, and P. M. Reis, *Proc. Natl. Acad. Sci. U.S.A.* **112**, 14 (2015).
- [33] J. C. Pàmies, A. Cacciuto, and D. Frenkel, *J. Chem. Phys.* **131**, 044514 (2009).
- [34] W. L. Miller and A. Cacciuto, *Soft Matter* **7**, 7552 (2011).
- [35] M. Zu, P. Tan, and N. Xu, *Nat. Commun.* **8**, 2089 (2017).
- [36] L. Landau and E. Lifshitz, *Theory of Elasticity* (Butterworth, Oxford, 1999).
- [37] S. Atkinson, F. H. Stillinger, and S. Torquato, *Proc. Natl. Acad. Sci. U.S.A.* **111**, 18436 (2014).
- [38] D. R. Nelson and F. Spaepen, *Solid State Physics* **42**, 1 (1989).
- [39] D. Wan and S. C. Glotzer, *Soft Matter* **14**, 3012 (2018).
- [40] D. R. Nelson, *Defects and Geometry in Condensed Matter Physics* (Cambridge University Press, Cambridge, 2002).
- [41] P. Chaikin and T. Lubensky, *Principles of Condensed Matter Physics* (Cambridge University Press, 1995), 1st ed.
- [42] G. van Anders, D. Klotz, N. K. Ahmed, M. Engel, and S. C. Glotzer, *Proc. Natl. Acad. Sci. U.S.A.* **111**, E4812 (2014).
- [43] T. O. E. Skinner, D. G. A. L. Aarts, and R. P. A. Dullens, *Phys. Rev. Lett.* **105**, 168301 (2010).
- [44] M. Girard, S. Wang, J. S. Du, A. Das, Z. Huang, V. P. Dravid, B. Lee, C. A. Mirkin, and M. Olvera de la Cruz, *Science* **364**, 1174 (2019).
- [45] M. Bowick, A. Cacciuto, D. R. Nelson, and A. Travesset, *Phys. Rev. Lett.* **89**, 185502 (2002).
- [46] R. E. Guerra, C. P. Kelleher, A. D. Hollingsworth, and P. M. Chaikin, *Nature* **554**, 346 (2018).
- [47] J. H. Conway, H. Burgiel, and C. Goodman-Strauss, *The symmetries of things* (AK Peters/CRC Press, 2016).
- [48] D. Struik, *Lectures on Classical Differential Geometry* (Dover Publications, New York, 1988), 2nd ed.
- [49] Z. Yao and M. Olvera de la Cruz, *Phys. Rev. Lett.* **111**, 115503 (2013).
- [50] V. Soni, L. R. Gómez, and W. T. M. Irvine, *Phys. Rev. X* **8**, 011039 (2018).
- [51] E. Jagla, *Phys. Rev. E* **58**, 1478 (1998).
- [52] T. Dotera, *Isr. J. Chem.* **51**, 1197 (2011).
- [53] T. Dotera, T. Oshiro, and P. Ziherl, *Nature* **506**, 208 (2014).
- [54] T. Narayanan and A. Kumar, *Phys. Rep.* **249**, 135 (1994).
- [55] Z. Yao, *Soft Matter* **13**, 5905 (2017).
- [56] C. N. Likos, *Soft Matter* **2**, 478 (2006).
- [57] N. Brodu, J. A. Dijksman, and R. P. Behringer, *Phys. Rev. E* **91**, 032201 (2015).